Progress In Electromagnetics Research M, Vol. 111, 89–101, 2022

A Dual-Band Ultra-Wideband Conformal Antenna for WCE

Maohai Ran[1], Ming Ye[2, *], and Bo Yin[2]

Abstract—In this paper, a dual-band ultra-wideband conformal antenna for Wireless Capsule Endoscopy is proposed. The antenna uses polyimide as a substrate of side wall to achieve conformality, leaving space for other components of the Wireless Capsule Endoscopy. The feeding network of the conformal antenna utilizes the circuit characteristics of Complementary Split-Ring Resonator to achieve dual-band operation at 1.4 GHz and 4.0 GHz. Based on the principle of wideband characteristics of spiral antennas, the conformal antenna radiation structure is improved. A short-pin is loaded at an appropriate position to improve the impedance matching of the antenna and achieve ultra-wideband without changing the resonant points of the antenna. The operating bandwidth of the antenna can reach 30.3% (1.20 $\sim$ 1.63 GHz) and 53.3% (3.33 $\sim$ 5.75 GHz), respectively. In addition, the antenna is placed in different simulation models to verify the stability of its operation. Minced pork is used to verify effectiveness of the conformal antenna. The measured results show that the proposed antenna is suitable for capsule endoscopy.

1. INTRODUCTION

Traditional gastroscopic examination adopts wired method, which usually brings strong discomfort to the patient. The advent of wireless capsule endoscopy systems (WCEs) has greatly improved patient comfort during inspections [1]. WCE integrates the required devices into a capsule, making wired inspections wireless. A conventional WCE contains battery, LED, camera, image sensor, and wireless transmission module [2]. The wireless transmission module is mainly composed of a capsule antenna [3]. Capsule antenna, which used to transmit date, is one of the key devices of WCE. According to the research of WCE antennas, there are mainly three different forms of capsule antennas at this stage, namely planar structure [4, 5], multilayer structure [6, 7], and surface conformal structure [8–12]. Among them, plane structure and multi-layer structure antennas occupy the internal space of the capsule, which is not conducive to the miniaturization of the entire system. The conformal antenna can attach metal to the inner wall of the capsule to improve space utilization, but it does not have a complete feeding ground plate structure and may be interfered by devices such as batteries in the actual application process. Therefore, in addition to the requirements of implantable antennas, the design of capsule antennas also needs to consider the shape characteristics of WCE.

There has been a lot of research on WCE antennas. A planar antenna that realizes miniaturized by loading slots on the radiator and the ground is proposed in [9]. At the same time, the impedance bandwidth of the antenna is expanded, and a relative bandwidth of 20.5% is achieved. In [10], a stepped monopole antenna is divided into three parts, which control different resonances respectively. Wideband is achieved through multiple resonant bands. Reference [11] introduced a symmetric double loop antenna. By adding two rectangular patches in the center of loop and rotating the feeding direction by 90°, an ultra-wideband (UWB) of 143% can be achieved in the ISM band. However, this antenna

Received 4 April 2022, Accepted 25 May 2022, Scheduled 21 June 2022

* Corresponding author: Ming Ye (2057299173@qq.com).

[1] Chongqing Electric Power College, Chongqing 400053, China. [2] School of Optoelectronic Engineering, Chongqing University of Posts and Telecommunications, Chongqing 400065, China.

has only one operating band and cannot achieve dual-modes of the device. Due to its conformal and wideband performance, the spiral antenna is often used in the design of WCE antennas [7, 12]. For example in [7], a wideband antenna with an impedance bandwidth of over 40% is proposed. The antenna radiates through a three-layer helix structure to extend the bandwidth. A dual-band conformal helical antenna is proposed in [12]. Two spiral arms are used to extend the current path for miniaturization. The antenna can achieve relative bandwidths of 39.2% and 12.1% at 2.4 GHz and 5.8 GHz.

With the advancement of medical technology, the demand for high-speed information transmission and real-time video transmission of the WCE is gradually increasing [13]. Wideband antenna can transmit a large amount of data, which is the best solution to the problem. At the same time, the wide operating bandwidth can improve the performance degradation caused by the frequency shift of the antenna. However, the single-band implantable antenna cannot support multiple operation modes of the implanted device. When the human body does not need the implanted device to work, one operation mode causes the limited battery energy to be wasted. At this time, if the device can be switched to sleep mode, the system power consumption can be reduced [14, 15]. In order to achieve this function, the WCE antenna needs to have multiple operating frequency bands.

The antenna proposed in this paper adopts the combination of conformal structure and planar feeding network. The radiation structure of antenna is attached to the polyimide (PI) substrate to achieve conformality. The antenna can operate in 1.4 GHz WMTS band and 4.0 GHz, the low frequency part of UWB band, with relative bandwidths of 30.3% and 53.3%, respectively. The antenna can be conformal to the inner wall of the capsule while supporting multiple operating modes of WCE and massive data transmission.

2. ANTENNA DESIGN AND ANALYSIS

2.1. The Structure of Antenna

The WCE antenna in this paper is shown in Fig. 1. The antenna consists of a feeding network and a conformal side wall, and is fed by a 50 Ω coaxial probe. The dielectric substrate of the bottom circular feeding network is Rogers RT/duroid 5880 with a thickness of 0.787 mm. As shown in Figs. 2(a) and (b), the upper surface of the feeding network is a copper wire used for connecting the conformal parts, and the bottom surface is a Complementary Split-Ring Resonator (CSRR) shaped defected ground structure (DGS) that excites the lower resonant part. The short-pin is used to match impedance and expand bandwidth. The expansion of the side conformal part is shown in Fig. 2(d). The flexible PI material with dielectric constant 3.5 and loss tangent angle 0.008 is used as the substrate, and the thickness is 0.1 mm. The length of the PI substrate is equal to the circumference of the bottom feeding network. The copper is attached to the inside of the PI substrate, and when the substrate is bent into a cylinder, the copper can form an improved spiral. The structural parameters of the antenna are shown in Table 1.

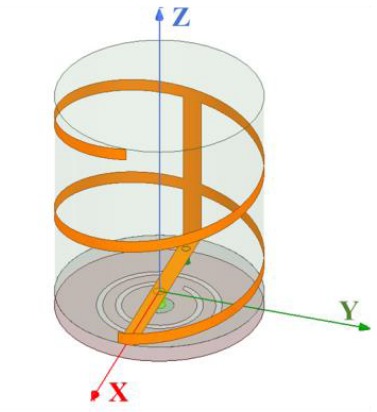

Figure 1. The WCE antenna.

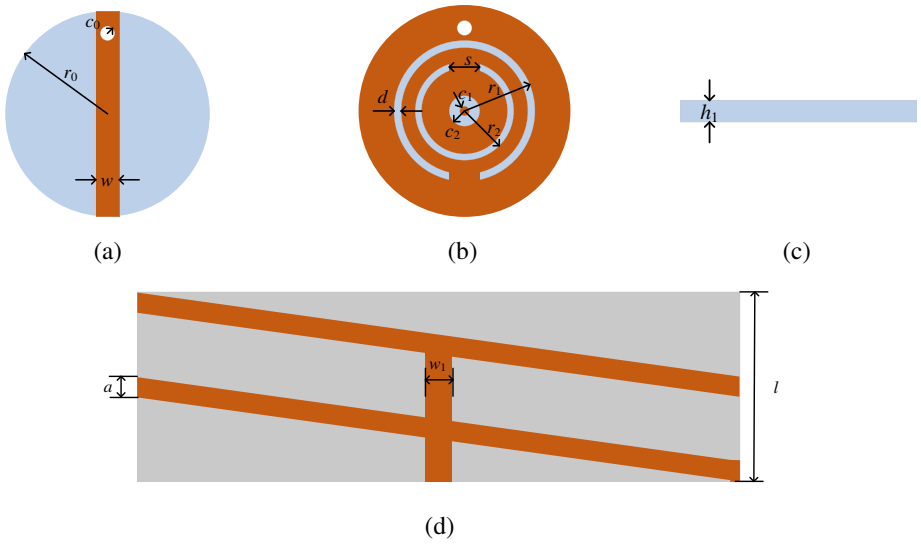

Figure 2. (a) The upper of the feeding network. (b) The bottom of the feeding network. (c) The side of the feeding network. (d) The expansion of antenna side wall.

Table 1. Geometrical parameters of the proposed antenna. (Units: mm).

Parameters	Values	Parameters	Values	Parameters	Values
l	11.0	s	1.2	c_1	0.3
w	0.8	d	0.3	c_2	0.7
r_0	5.0	r_1	3.0	w_1	0.9
c_0	0.2	r_2	2.1	a	0.6

The biggest difference between implantable antennas and ordinary antennas is the operating environment. The human body is a complex system consisting of many different tissues and organs. Various biological tissues have not only different shapes, but also different electromagnetic parameters. The values of electromagnetic parameters related to human tissue are mainly based on the measurement data of Gabriel et al. [16–18]. To analyze the performance and sensitivity of the proposed antenna, a simulation model as shown in Fig. 3 is set up in HFSS (High Frequency Structure Simulator). They

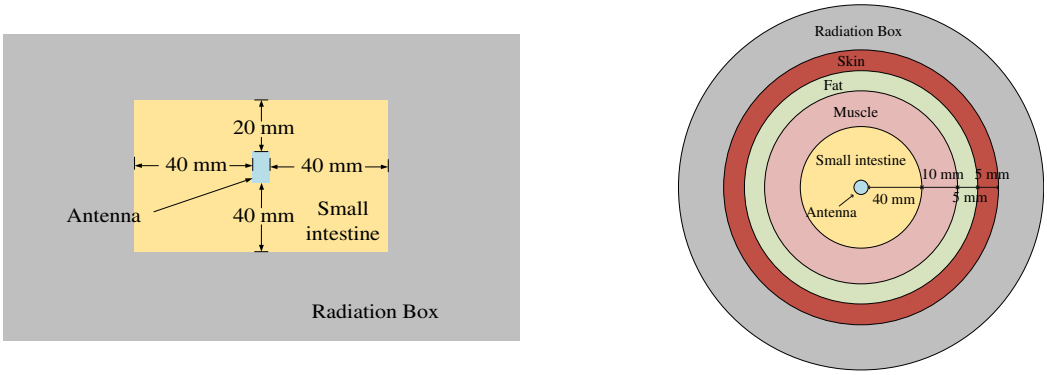

(a) The small intestine model

(b) The four-layer model

Figure 3. Antenna simulation environment in HFSS.

are the small intestine model shown in Fig. 3(a) and the four-layer model (skin, fat, muscle, and small intestine) shown in Fig. 3(b), respectively.

The S_{11} of antenna in two environments are shown in Fig. 4. The antenna resonates at 1.4 GHz and 4.0 GHz and operates in $1.20 \sim 1.63$ GHz and $3.33 \sim 5.75$ GHz in model (a). The impedance matching bandwidths are 30.3% and 53.3%, respectively, which meet the requirements of UWB antenna. Fig. 4 shows that there is little difference between the simulation results in two models. In model (b), the resonant point of the antenna shifts to the low-frequency direction, and the bandwidth will decrease slightly, but it can still cover WMTS band and the low frequency part of UWB. The S_{11} in two models coincide roughly, which proves that the antenna operates stably.

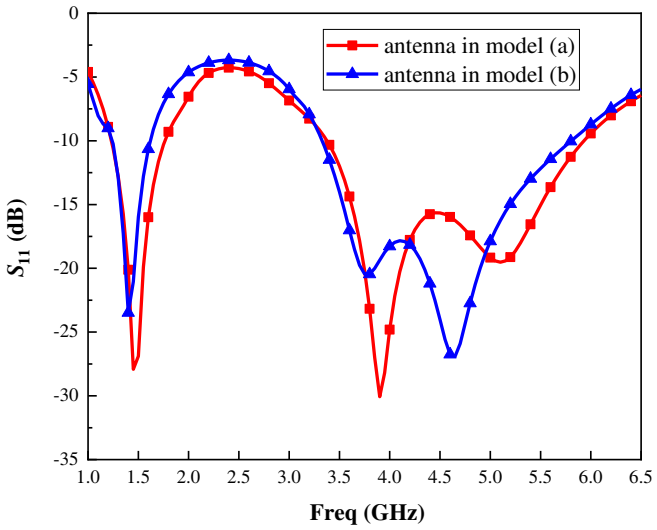

Figure 4. The S_{11} in two environments.

Figures 5 and 6 show the radiation pattern of the antenna in small intestine model. The peak gain of the antenna is -35.0 dBi at 1.4 GHz and -29.9 dBi at 4.0 GHz. The radiation pattern of the antenna basically maintains the same at different points of the two operation bands. Although the radiation pattern of the antenna changes in the high frequency band, it may be caused by the wideband. The radiation patterns show the stability of the WCE antenna. Table 2 shows the main performance parameters of the WCE antenna in two models, including bandwidth and peak gain. It can be seen from the data in Fig. 4 and Table 2 that the resonant frequency points of the antenna are very close in the two models. The impedance bandwidth in the 4 GHz band is reduced in model (b). The gain is lower in the four-layer model than in the muscle model.

Table 2. Antenna performance implanted in two models. ($f_l = 1.4$ GHz, $f_h = 4.0$ GHz).

Model	Bandwidth (%)		Gain (dBi)	
	f_l	f_h	f_l	f_h
Small intestine	30.3	50.3	-35.0	-29.9
Four-layer	36.1	39.7	-36.8	-30.3

2.2. Dual-Band Performance Analysis

In order to achieve dual-band effect of the WCE antenna, the CSRR DGS as shown in Fig. 7(a) is loaded into the antenna feeding network. The equivalent circuit of CSRR is shown in Fig. 7(b).

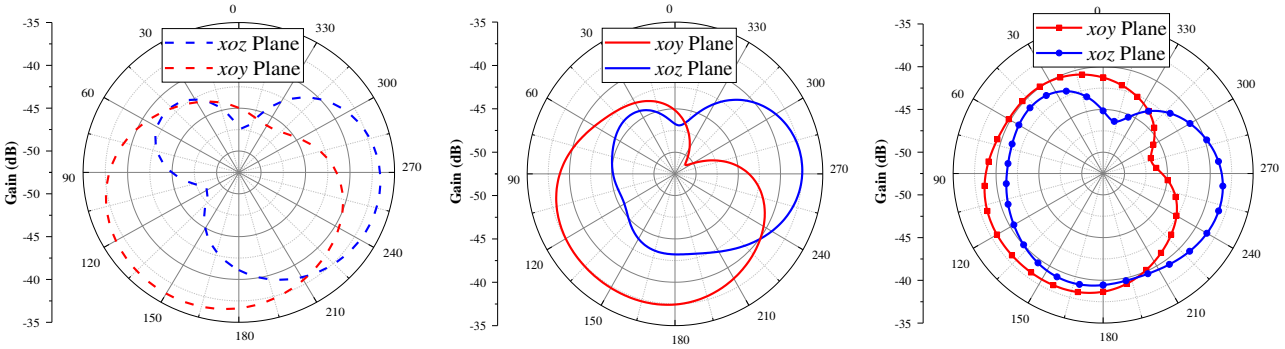

(a) 1.2 GHz (b) 1.4 GHz (c) 1.6 GHz

Figure 5. The Radiation pattern at 1.2 GHz, 1.4 GHz and 1.6 GHz.

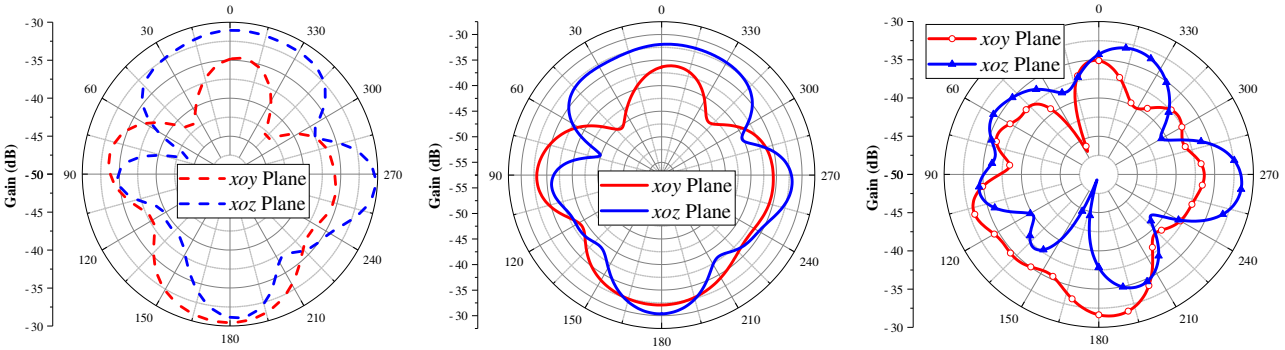

(a) 3.3 GHz (b) 4.0 GHz (c) 5.7 GHz

Figure 6. The Radiation pattern at 3.3 GHz, 4.0 GHz and 5.7 GHz.

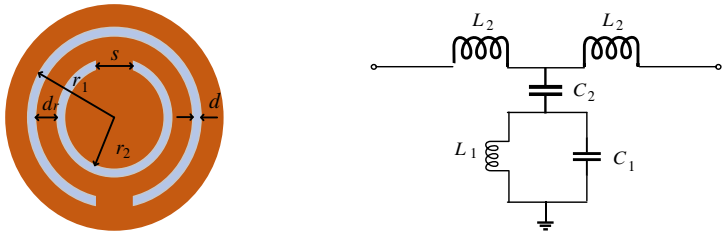

(a) (b)

Figure 7. The CSRR DGS loaded in feeding network. (a) The structure of CSRR. (b) The equivalent circuit.

According to the theory of CSRR, its resonant frequency is related to the inner and outer ring distance d_r and the ring radius. The formula can be expressed as follows [19]:

$$f_{\text{CSRR}} = \frac{c}{2\pi}\sqrt{\frac{r_1 - r_2}{(\varepsilon_r + 2)\left[r_1 - 2d_r - (r_1 - r_2 - d_r)\right]^3}} \tag{1}$$

where ε_r is the dielectric constant of substrate; r_1 and r_2 are radii of outer and inner rings, respectively. Through calculation and simulation, the resonant points of CSRR are related to each parameter. However, when the WCE antenna loads CSRR DGS, its resonant point will shift, and it is necessary to design the feeding network and WCE antenna together to determine the final structure parameters.

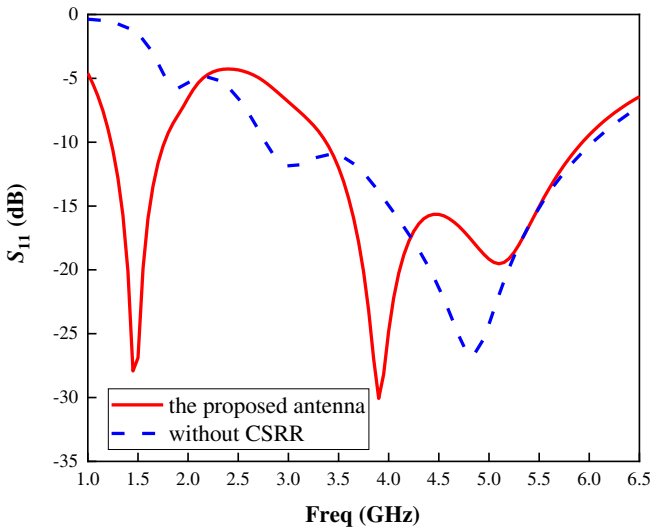

Figure 8. The S11 of WCE antenna before and after loading CSRR DGS.

The S_{11} of the WCE antenna loaded CSRR DGS is shown in Fig. 8. As can be seen from the figure, loading CSRR DGS has little effect on the working bandwidth of 4 GHz, but a new resonant point is introduced at 1.4 GHz, making the WCE antenna have dual-band characteristics.

Figure 9 shows the VSWRs and impedances of WCE antenna before and after loading CRSS DGS. After loading the CSRR DGS, the VSWR of the antenna changes little at 4.0 GHz, but decreases to less than 1.5 at 1.4 GHz. At the same time, the real part of the antenna input impedance shown in Fig. 9(b) is close to the matching impedance of 50 Ω at 1.4 GHz, indicating that a new resonance point has appeared. Fig. 9 verifies that loading CSRR DGS on the feeding network grounding plate can add a new resonant point to achieve dual-band operation of WCE antenna.

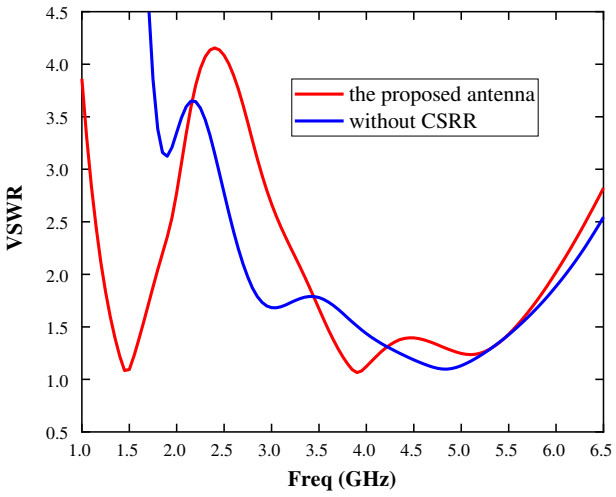

(a) VSWR

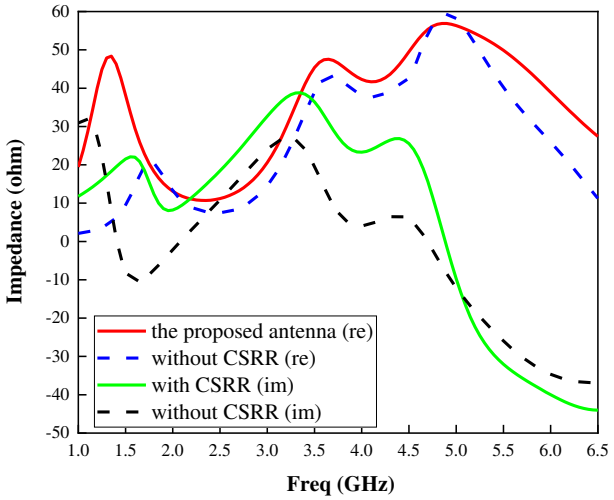

(b) Impedance

Figure 9. The VSWR and impedance of WCE antenna before and after loading CRSS DGS.

2.3. Wideband Performance Analysis

Through the introduction of antenna structure, it can be known that the radiation structure of WCE antenna is a spiral when the short-pin and feeding network are not loaded. Spiral antenna is an axial

mode antenna, with the radiation energy along the axial direction. The impedance of antenna remains constant over a wide range of bands so that spiral antenna has wideband performance. In order to expand bandwidth, a short-pin is loaded in feeding network. The current distribution will not change when a short-pin is loaded at the zero potential point of the feeding network, but the antenna size can be miniaturized. At the same time, the loading of the short-pin is equivalent to introducing inductance elements into the microstrip line, which is used to offset capacitive impedance of the antenna and to expand bandwidth.

The S_{11} of the WCE antenna with loaded short-pin is shown in Fig. 10. After loading the short-pin, the 1.4 GHz band introduced by the CSRR defect does not change much, but the 3.5 GHz band excited by the spiral structure shifts to higher frequency, and the impedance bandwidth becomes wider. Fig. 11 shows the VSWRs and impedances of WCE antenna before and after loading short-pin. The short-pin reduces the VSWR of the antenna at 4 GHz and remains below 1.5 in the wider band. Meanwhile, the impedance of WCE antenna remains stable at high frequency. Fig. 11 indicates that the matching of WCE antenna is better at high frequency, which further verifies the effectiveness of loading short-pin to expand bandwidth.

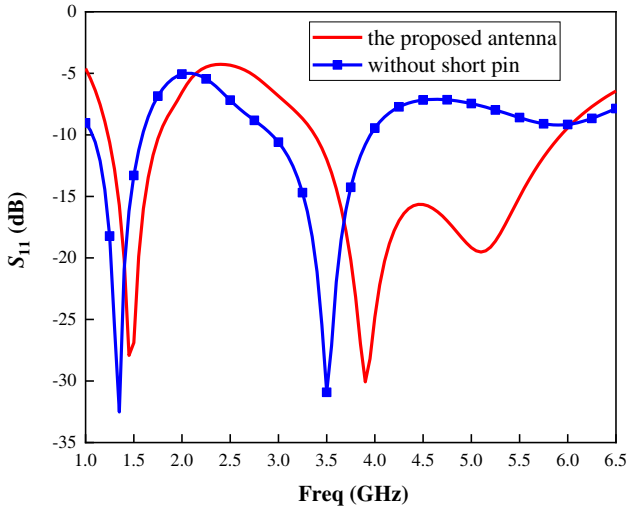

Figure 10. The S_{11} of WCE antenna before and after loading short-pin.

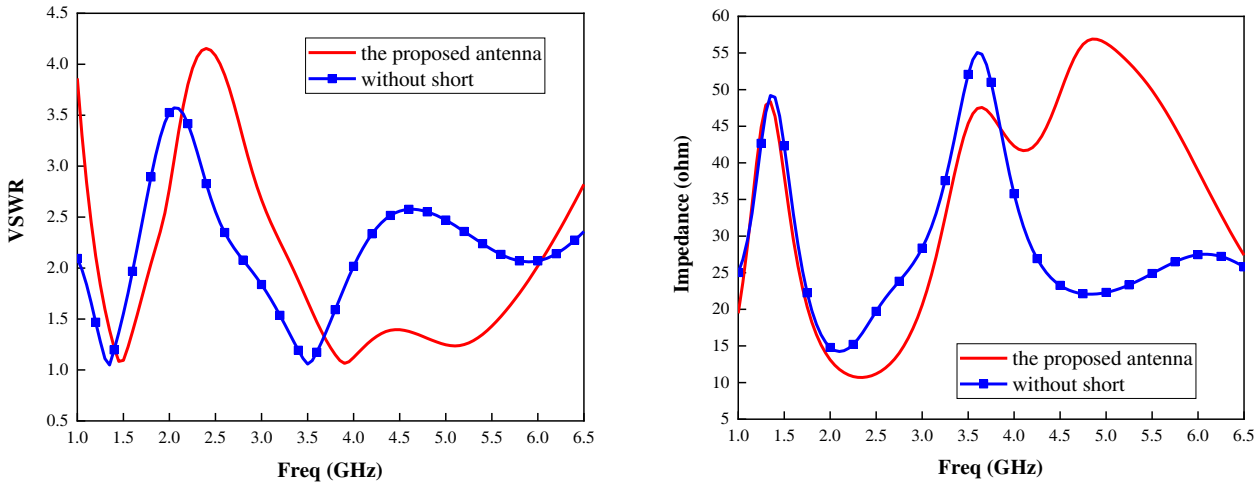

Figure 11. The VSWR and impedance of WCE antenna before and after loading short-pin.

2.4. 24 SAR Distribution and Wireless Communication Link Margin

In the design of implantable antenna, the specific absorption rate (SAR) is usually used to measure the safety of the antenna operating inside human body. The SAR distributions of the proposed WCE antenna in two models are shown in Fig. 12. The relevant data are listed in Table 3. Assuming an input power of 1 W, the maximum average SARs (1 g tissue) are 742 and 527 W/kg in the small intestine model, and 761 and 454 W/kg in four-layer model at 1.4 GHz and 4 GHz, respectively. To reach the IEEE-specified human safety level limit of 1.6 W/kg, the maximum allowable input powers for small intestine model and four-layer model are 2.12 mW and 2.05 mW. The maximum allowable input power is much higher than the output power of actual commercial transmitters [20].

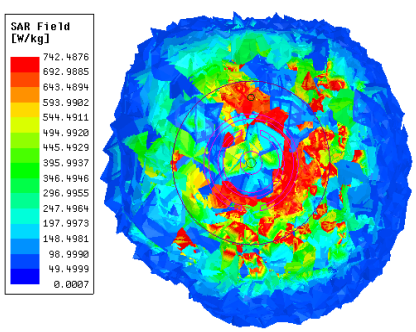

(a) 1.4 GHz in small intestine model

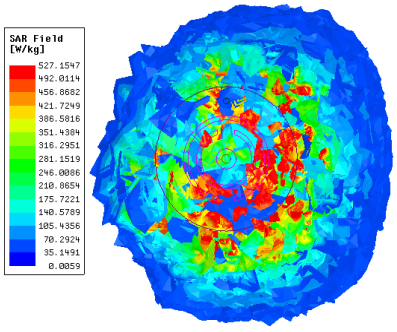

(b) 4 GHz in small intestine model

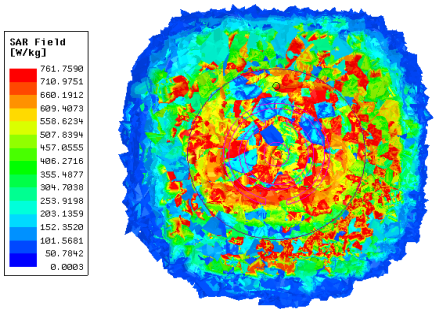

(c) 1.4 GHz in four-layer model

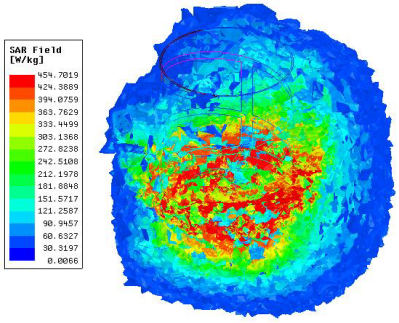

(d) 4 GHz in four-layer model

Figure 12. SAR distribution of the WCE antenna.

Table 3. The relevant data of SAR and input power. ($f_l = 1.4\,\text{GHz}$, $f_h = 4\,\text{GHz}$).

Model	SAR (W/kg)		maximum input power (mW)
	f_l	f_h	
Small intestine	742	527	2.12
Four-layer	761	454	2.05

The link margin of the WCE antenna is analyzed to evaluate the communication capability. According to Friis Transmission Formula, the link margin for far-field wireless communication is calculated as follows [21]:

$$\begin{aligned}\text{Link Margin (dB)} &= Link\frac{C}{N_0} - Requied\frac{C}{N_0} \\ &= (P_t + G_t - L_f + G_r - N_0) - \left(\frac{E_b}{N_0} + 10\log_{10} B_r - G_c + G_d\right) \end{aligned} \quad (2)$$

$$L_f(\text{dB}) = 20\log_{10}\left(\frac{4\pi d}{\lambda}\right) \tag{3}$$

$$N_0 = 10\log_{10} k + 10\log_{10} T \tag{4}$$

where P_t is the transmitting power; L_f is the path loss; d is the distance between the transmitting and receiving antennas; G_t and G_r are gains of transmitting antenna and receiving antenna; N_0 is the noise power density; and B_r represents the bit rate. BPSK modulation mode is selected, and impedance mismatch loss is ignored. The relevant parameters for calculating the link margin of the proposed WCE antenna are shown in Table 4.

Table 4. Communication link margin-related parameters.

Frequency (GHz)	1.4	4
Tx power (dBm)	−30	−25
Tx antenna gain G_t (dBi)	−36.8	−30.3
Rx antenna gain G_r (dBi)	2.15	
Boltzmann constant k	1.38×10^{-23}	
Ambient temperature T (K)	293	
Noise power density N_0 (dB/Hz)	−199.95	
E_b/N_0 (ideal PSK) (dB)	9.6	
Coding gain G_c (dB)	0	
Fixing deterioration G_d (dB)	2.5	

In this paper, in order to achieve reliable communication, a link margin of 10 dB is reserved. The link margin analysis of the WCE antenna at the two resonance points is shown in Fig. 13. As can be seen, the farthest transmission distance of the WCE antenna is about 6.4 m at 1.4 GHz and 3.8 m at 4.0 GHz.

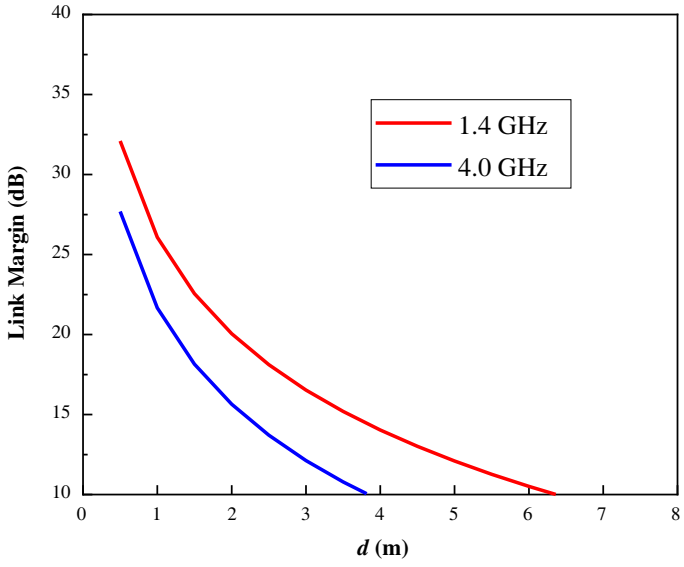

Figure 13. Link margin with different frequency points.

3. FABRICATION AND MEASUREMENT

In order to verify the effectiveness of the antenna, the WCE antenna is fabricated and measured. The feeding network and side wall are shown in Fig. 14(a). Fig. 14(b) shows the comparison between the complete antenna welded by the two parts and the capsule. It is obvious that the antenna size is small and can be applied in the WCE system. The measuring device of antenna is shown in Fig. 14(c). The antenna is measured in minced pork, which is selected to replace small intestine tissue. As shown in Fig. 14(c), a 10 cm RF adapter is used to extend the feed port of the WCE antenna. Then put the antenna into 5 cm thick minced pork tissue to measure.

(a) The side wall and feeding network

(b) The WCE antenna

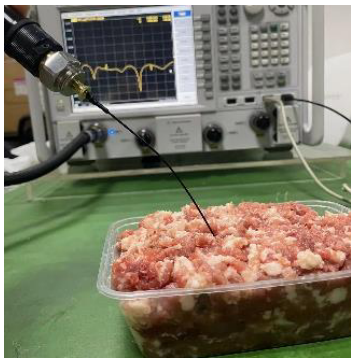

(c) The antenna in pork

Figure 14. Fabricated antenna and measurement setup.

Figure 15 shows the comparison of the measured and simulated results of the WCE antenna. The resonant frequency of the antenna is slightly shifted in pork, and the operating bandwidth becomes wider. The reason of measurement errors is summarized as follows. First, the welding of antenna may change the size of the patch structure, which may excite new resonance points. Second, the antenna uses a flexible substrate with a small size, which is easy to be squeezed and deformed when being placed in pork for measurement, so the test results are easy to be affected. Third, the short-pin is replaced by a metal via during fabrication, which may cause new errors during measurement. Compared with the simulation results, there are small errors in the measured result of the antenna, but the resonant points are basically consistent, and the operating bandwidth can cover the WMTS band and low frequency part of UWB.

In order to measure the pattern of the antenna, the far field measurement of the WCE antenna is carried out in an anechoic chamber. Similarly, the minced pork is used to replace small intestine tissue, as shown in Fig. 16.

The comparison of simulation and measurement is shown in Fig. 17. The gain of WCE antenna in pork is larger than the simulation result. The reason may be that the direction of the antenna

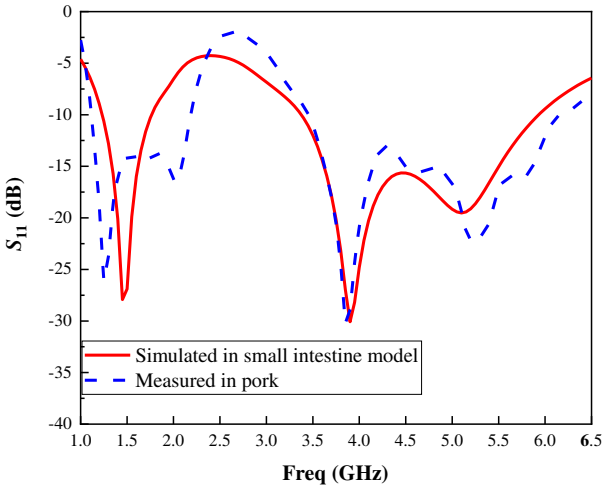

Figure 15. Comparison of simulation and measurement in liquid.

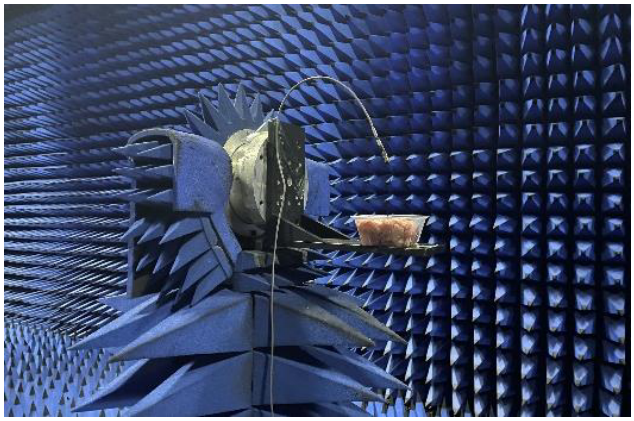

Figure 16. Far field measurement of antenna.

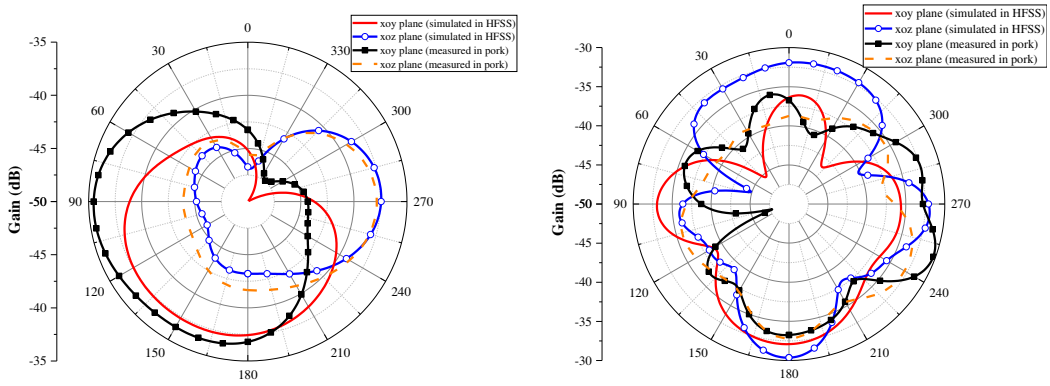

(a) 1.4 GHz (b) 4.0 GHz

Figure 17. Comparison of simulation and measurement in pork.

Table 5. Proposed antenna comparison with others.

Ref.	Freq (MHz)	Bandwidth (%)	Gain (dBi)	Model
[8]	402	236.2	−29.7	Muscle
	915	104	−28.7	
	2400	55.4	−20.8	
[10]	2450	31.6	−44.5	Small intestine
[11]	2450	143.0	−12.6	Muscle
[12]	2400	39.2	−35.2	Three-layer (fat, muscle,
	5800	12.1	−28.1	mucosa membrane)
[13]	433	102.1	−30.6	Multiple-layer (skin, fat,
	1400	23.7	−19.9	muscle, gastrointestinal)
[14]	915	21.6	−35.0	Small intestine
This work	1400	30.3	−36.8	Four-layer (skin, fat,
	400	53.3	−30.3	muscle, small intestine

placed in pork is unstable. The size of the antenna is very small, and the position cannot be accurately determined during measurement, so that it does not correspond to the horn antenna, which results in errors in the measurement results.

4. CONCLUSION

A dual-band wideband WCE antenna is proposed in this paper. The antenna uses PI as a substrate to realize conformal design and leave space for other devices of a WCE system. The antenna uses the improved spiral structure as the main radiator. The short-pin is loaded to offset the capacitance and to achieve good matching and wideband operation in the low frequency part of UWB. The relative bandwidth reaches 30.3% and 53.3% in two bands. A CSRR DGS is loaded on the feeding network, so that a new operating band is added by its circuit characteristics. The WCE antenna operates in WMTS band and the low frequency part of UWB. Through the calculation of SAR and link margin, the maximum input power and communication distance of the WCE antenna in two bands are analyzed. The WCE antenna is fabricated and placed in pork for measurement. The measured results are in good agreement with the simulation ones. Comparison of our work with previously designed conformal WCE antennas can be found in Table 5. Results indicate that the proposed antenna has good performance balance among dual-bands, bandwidth, and gain.

ACKNOWLEDGMENT

This work was supported by the Chongqing Graduate Research and Innovation Project (CYS20265).

REFERENCES

1. Iddan, G., G. Meron, A. Glukhovsky, et al., "Wireless capsule endoscopy," *Nature*, Vol. 405, 417–418, 2000.
2. Glukhovsky, A., "Wireless capsule endoscopy," *Sensor Review*, Vol. 23, No, 2, 128–133, 2003.
3. Malik, N. A., P. Sant, T. Ajmal, and M. Ur-Rehman, "Implantable antennas for bio-medical applications,"*IEEE Journal of Electromagnetics, RF and Microwaves in Medicine and Biology*, Vol. 5, No. 1, 84–96, 2021.
4. Hayat, S., S. A. A. Shah, and H. Yoo, "Miniaturized dual-band circularly polarized implantable antenna for capsule endoscopic system," *IEEE Trans. Antennas Propag.*, Vol. 69, No. 4, 1885–1895, 2021.
5. Yun, S., K. Kim, and S. Nam, "Outer-wall loop antenna for ultrawideband capsule endoscope system," *IEEE Antennas and Wireless Propagation Letters*, Vol. 9, 1135–1138, 2010.
6. Lee, S. H., J. Lee, Y. J. Yoon, et al., "A wideband spiral antenna for ingestible capsule endoscope systems: Experimental results in a human phantom and a pig," *IEEE Transactions on Biomedical Engineering*, Vol. 58, No. 6, 1734–1741, 2011.
7. Liu, C., Y. X. Guo, and S. Q. Xiao, "Circularly polarized helical antenna for ISM-band ingestible capsule endoscope systems," *IEEE Trans. Antennas Propag.*, Vol. 62, No. 12, 6027–6039, 2014.
8. Basir, A., M. Zada, Y. Cho, et al., "A dual-circular-polarized endoscopic antenna with wideband characteristics and wireless biotelemetric link characterization," *IEEE Trans. Antennas Propag.*, Vol. 68, No. 10, 6953–6963, 2020.
9. Cui, W., R. Liu, L. Wang, et al., "Design of wideband implantable antenna for wireless capsule endoscope system," *IEEE Antennas and Wireless Propagation Letters*, Vol. 18, No. 12, 2706–2710, 2019.
10. Li, R., Y. X. Guo, and G. Du, "A conformal circularly polarized antenna for wireless capsule endoscope systems," *IEEE Trans. Antennas Propag.*, Vol. 66, No. 4, 2119–2124, 2018.
11. Shang, J. L. and Y. Yu, "An ultrawideband capsule antenna for biomedical applications," *IEEE Antennas and Wireless Propagation Letters*, Vol. 18, No. 12, 2548–2551, 2019.

12. Liu, K., R. P. Liu, W. J. Cui, et al., "Design of conformal spiral dual-band antenna for wireless capsule system," *IEEE Access*, Vol. 9, 117349–117357, 2021.
13. Wang, M. J., P. Ma, L. L. Cai, et al., "Investigation of localizing precise human abdomen models for wireless capsule endoscopy antenna design," *IEEE Trans. Antennas Propag.*, Vol. 70, No. 2, 1367–1379, 2022.
14. Das, R. and H. Yoo, "A wideband circularly polarized conformal endoscopic antenna system for high-speed data transfer," *IEEE Trans. Antennas Propag.*, Vol. 65, No. 6, 2816–2826, 2017.
15. Shah, I. A., M. Zada, and H. Yoo, "Design and analysis of a compact-sized multiband spiral-shaped implantable antenna for scalp implantable and leadless pacemaker systems," *IEEE Trans. Antennas Propag.*, Vol. 67, No. 6, 4230–4234, 2019.
16. Gabriel, C., S. Gabriel, and E. Corthout, "The dielectric properties of biological tissues: I. Literature survey," *Physics in Medicine and Biology*, Vol. 41, No. 11, 2231–2249, 1996.
17. Gabriel, S., R. W. Lau, and C. Gabriel, "The dielectric properties of biological tissues: II. Measurements in the frequency range 10 Hz to 20 GHz," *Physics in Medicine and Biology*, Vol. 41, No. 11, 2251–2269, 1996.
18. Gabriel, S., R. W. Lau, and C. Gabriel, "The dielectric properties of biological tissues: III. Parametric models for the dielectric spectrum of tissues," *Physics in Medicine and Biology*, Vol. 41, No. 11, 2271–2293, 1996.
19. Yousfi, A., A. Lamkaddem, K. A. Abdalmalak, et al., "A miniaturized triple-band and dual-polarized monopole antenna based on a CSRR perturbed ground plane," *IEEE Access*, Vol. 9, 164292–164299, 2021.
20. Yin, B., M. Ye, J. H. Cong, and Y. Xu, "A miniaturized dual-band circularly polarized implantable antenna by half-cutting," *Progress In Electromagnetics Research M*, Vol. 108, 139–149, 2022.
21. Xia, W., K. Saito, M. Takahashi, and K. Ito, "Performances of an implanted cavity slot antenna embedded in the human arm," *IEEE Trans. Antennas Propag.*, Vol. 57, No. 4, 894–899, 2009.